Characterisation of barrel swirl motion under steady flow conditions

Baker, P. , Benjamin, S.F. , Girgis, N.S. , Newman, A.W. and Seeley, W.A.

SAE TECHNICAL PAPER SERIES

950729

Characterisation of Barrel Swirl Motion Under Steady Flow Conditions

P. Baker, S. F. Benjamin, N. S. Girgis, A. W. Newman, and W. A. Seeley
Coventry Univ.

The Engineering Society For Advancing Mobility Land Sea Air and Space®
INTERNATIONAL

International Congress and Exposition
Detroit, Michigan
February 27 - March 2, 1995

400 Commonwealth Drive, Warrendale, PA 15096-0001 U.S.A. Tel: (412)776-4841 Fax:(412)776-5760

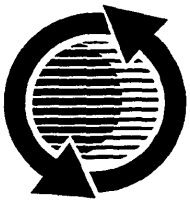

ISSN 0148-7191

Printed in USA 90-1203D/PG

950729

Characterisation of Barrel Swirl Motion Under Steady Flow Conditions

P. Baker, S. F. Benjamin, N. S. Girgis, A. W. Newman, and W. A. Seeley
Coventry Univ.

ABSTRACT

The purpose of this paper is to characterise the flow field through the inlet valves, and tumble to swirl conversion tube of a steady state flow rig using HWA. LDA and CFD techniques. Three cylinder head configurations were developed which were found to produce three levels of barrel swirl motion. The swirl precesses around the central core of the conversion tube at all degrees of swirl. Varying degrees of swirl produced differing axial velocity profiles, and flow reversal occurred in the central core of the conversion tube for the high swirling case. The results obtained for this study indicate that care must be exercised when deducing the barrel swirl ratio for real engines from steady flow rig analysis.

INTRODUCTION

Due to environmental and consumer requirements there has been an increasing need to design and develop combustion chambers that reduce exhaust emissions and improve fuel economy in spark ignition (S.I.) engines. This requirement has been amplified by the introduction of emissions standards with the Ultimate aim of reducing emissions to zero within the foreseeable future [1]*.

At Coventry University a programme is underway to study the development and breakdown of barrel swirl in spark ignition (S.I.) engines for improved fuel economy and reduced exhaust emissions. The barrel swirl concept has been described by Benjamin [2]. The concept involves inducing a barrel or tumbling swirl motion within the cylinder. which comprises an organised air motion rotating about an axis perpendicular to the cylinder axis. During compression the vortex spins up until near the time of ignition where the large shear stresses convert the tumbling motion into turbulent energy. The control of the level of swirl and its breakdown is believed to be a function of the porting arrangements and chamber shape [3]. This programme of work is undertaken to develop a deeper understanding of these controlling parameters.

This paper reports on measurements made on a steady flow rig, the specific objectives of which are to:

a) Develop intake ports for inducing barrel swirl.

b) Quantify barrel swirl in real engines at inlet valve closure (IVC).

c) Provide inlet boundary conditions and validation data for CFD predictions.

It should be noted that steady flow rigs have been used extensively as part of the development procedure for conventional two valve engines. More recently Chapman [4] and Arcoumanis [5] have also used them for quantifying swirl in barrel swirl chambers.

EXPERIMENTAL SYSTEM

CYLINDER HEAD CONFIGURATIONS - Three cylinder head arrangements were used for the analysis of steady state engine flows. The first cylinder head arrangement can be seen in figure 1. It consists of a flat cylinder head with two straight inlet ports of 26mm diameter. To ensure a strong tumbling motion within the cylinder whilst still retaining a simplistic design the tubes were shrouded through 180°. The valve lift measurement was achieved by placing slip gauges between a fixed position on the inlet ports and the cylinder head.

The second and third cylinder head arrangements are similar in design, with a slight modification to the inlet ports for the third system. They are of a four valve pent roof chamber design (figure 2). The cylinder head was modified by inserting 30mm ramps into the intake tracts. The 30mm inserts have a tubular cross section, with a 180° (semi circular) ‘ramp’ attached to divert the airflow over the top of the inlet valves to produce a stronger in-cylinder tumbling motion. For the pent roof chamber, the inlet valve has a diameter of 32mm, with a maximum valve lift of 8.7mm.

STEADY STATE FLOW SYSTEM - The steady flow tests were undertaken on the flow rig shown schematically in Figure 3. The system was attached to the suction side of a centrifugal fan and air was drawn through, using a similar approach to Arcoumanis[5]. A Ricardo viscous flow air meter connected to an Airflow Developments single limb water manometer was used to measure the mass flowrate through the system. The inlet plenum chamber (diameter. 220mm, length 440mm) upstream of the test section was used to provide the upstream

* Numbers in square brackets designate references.

stagnation pressure necessary for discharge coefficient calculations. The downstream static pressure tapping is located in the tumble to swirl conversion tube, 504 mm from the centre of the cylinder. The pressure difference across the test section is defined as the difference between the upstream stagnation and downstream static pressure, and was measured by a single limb water manometer. This pressure difference remained constant throughout all tests, and was controlled by a ball valve attached to the outlet plenum chamber.

The 84 mm bore perspex cylinder has a length of 98mm which is 9mm below the motored engine BDC piston position. This permitted fitting of the tumble to swirl conversion tube (diameter 84mm). whilst providing confinement of the valve flow. The LDA measurement planes are located at 84, 168 and 252 mm along the conversion tube. which arc one, two, and three bore diameters respectively (see figure 4). The tumble to swirl conversion tube is a total of 546 mm in length. A piston crown, which is crucial for the development of the in-cylinder tumbling motion, is simulated by a flat plate placed at the bottom of the cylinder.

To assess the ability of the rig to maintain a steady flow, the pressures in both plenum chambers were measured independently, and the LDA system was used to measure a time history of the flow at several locations within the tumble to swirl conversion tube. Both analyses showed no unusual fluctuations in the flow.

HOT WIRE ANEMOMETRY - A lack of optical access around the inlet valve curtain area necessitated the use of hot wire anemometry to measure the velocity profiles around the inlet valve periphery. The system is a constant temperature anemometer and consists of a DISA type 55P11 90/10 platinum/rhodium single, wire probe connected to a DISA 55M10 CTA standard bridge and 55M01 main unit. The output signal from the bridge was fed into a DISA 55D31 DC voltmeter to obtain mean voltages.

HWA Resolving Method - To obtain the axial (U_a), radial (U_r), and tangential (U_t) velocity components around the valve curtain area the hot wire was placed in a plane parallel to the valve face and rotated to the three orientations (0°, 45°. 90°) shown in figure 5. At each orientation, the instantaneous effective cooling velocity (U_e) is assumed to be related to the instantaneous velocity components by the equation.

$$U_e^2 = U_x^2 \, U2x + k_2 U_y^2 + U_z^2 \quad \ldots (1)$$

where k is the yaw factor, and U_x, U_y, and U_z are components of velocity in a frame of reference attached to the wire as shown in figure 5.

To obtain the tangential, radial, and axial mean velocity components (U_t, U_r, U_a), a method similar to Catania[7] was used. By resolving equation (1) for the 0°, 45°, and 90° wire orientations and time averaging, a series of equations for U_t, U_r, and U_a can be achieved. These are,

$$U_t = \left(\frac{1}{2} K_1 + \left(\frac{1}{4} K_1^2 + K_2^2 \right)^{\frac{1}{2}} \right)^{\frac{1}{2}}$$

$$U_a = \left(K_3 - U_t^2 \left(1 + k^2 \right) \right)^{\frac{1}{2}}$$

$$U_r = \left(U_t^2 - K_1 \right)^{\frac{1}{2}}$$

where.

$$K_1 = \frac{1}{1 - k^2} \left(U_{e0}^2 - U_{e90}^2 \right)$$

$$K_2 = \frac{1}{2\left(1 - k^2\right)} \left(2U_{e45}^2 - U_{e0}^2 - U_{e90}^2 \right)$$

$$K_3 = \frac{1}{1 - k^2} \left(U_{e0}^2 - k^2 U_{e90}^2 \right)$$

and k = Yaw Factor

$U_{e0.}$ $Ue_{45.}$ and U_{e90} are the mean effective cooling velocities for the 0°,45°, and 90° wire orientations respectively.

Using this resolving method it is possible to determine not only velocity magnitude, but also direction. It can also be shown that $K_2 = - U_r U_t$ so if the radial component of velocity is assumed to be always positive, i.e. radially outwards from the valve, it is possible to determine the direction of the tangential velocity component.

Accuracy - The accuracy of the HWA technique and resolving method was assessed by placing the hot wire in arbitrary orientations and with various velocities relative to a known flow field on the calibration rig. This accuracy analysis also includes assumptions made during the calibration of the hot wire such as assuming the yaw factor to remain constant and the pitch factor being unity. The actual velocities were measured using the pitot tube. whilst the HWA measured velocities were obtained using the velocity resolving method described earlier. The three velocity components obtained from the HWA technique were then resolved to give a single velocity magnitude and direction. From these results it was found that the velocity magnitude could be measured to an accuracy of within 5%. whilst the direction could be measured to within 5°.

LASER DOPPLER ANEMOMETRY - LDA was used to measure the axial and swirl velocity, profiles at the measuring planes in the tumble conversion tube. This was preferable over HWA due to the unintrusive nature of the LDA technique. Figure 6 shows the basic arrangement of the single component fibre optic LDA system. which consists of (a) 3 Watt Spectraphysics, series 2000 Argon-Ion laser. (b) an optical unit incorporating miniature optics for beam splitting and Bragg cells for frequency shifting. and (c) a fibre-optically linked transmission and receiving probe. Table 1 details the specifications of the LDA system. The system was operated in back scatter where the light was scattered by particles of Titanium Dioxide (TiO_2), The TiO_2 seeding was supplied from an air jet atomiser into the inlet plenum chamber, which created an average particle diameter of 0.3 to 0.5 microns. The output

from the photo multiplier tube was processed by a burst correlator (TSI IFA750) interfaced to a rotating machinery resolver (TSI 1989) and a PC.

Wavelength	**514 nm**
Beam separation	**8 mm**
Focal length	**50 mm**
Beam intersection at half angle	**4.57°**
Measuring volume width	**0.122 mm**
Measuring volume length	**1.52 mm**
Calibration constant	**3.23 ms^{-1}/MHz**
Frequency shift	**10 MHz**

Table 1 - *Specifications of LDA system*

Accuracy - There are numerous sources of experimental error associated with the LDA technique[8]. The main sources are velocity gradient broadening, velocity biasing, and uncertainties from using a finite sample size when performing averages. To determine whether the errors affect the arithmetic averaging, the worst case scenario was chosen. This is where there are large velocity gradients in the flow, and the rms fluctuations are the greatest. At these points the flow statistics for mean velocity and turbulent velocity fluctuations were observed and no unusual deviations from a normal distribution using 1000 data points were detected. An additional test was also conducted where the averaging was biased by transit time methods. Tests for finite sample size, which also effect averages, were conducted. These were achieved by doubling the number of data points collected by the signal processor. No significant changes in the results were observed which confirmed that 1000 data points was statistically reasonable. Repeatability studies were also undertaken which encompassed all experimental errors associated with this analysis. It was estimated from the results that the single component velocities could be measured to an accuracy of within 10%.

RESULTS

The shrouded valve disc head was tested at a constant pressure drop of 200mm/H_2O across the test section to ensure a fully turbulent flow through the inlet port was achieved. This was used to assess the ability of the CFD code to cope with turbulent flow regimes, and has been reported in an earlier paper by the authors [6]. This pressure drop equates to an equivalent engine speed of 1900rpm. In order to keep the steady flow analysis consistent with measurements conducted on motored engines by the authors [9], a pressure drop of 64mm/H_2O was chosen which simulates an engine speed of 1000rpm. The equivalent engine speed was calculated from the mass flow rate data collected at each valve lift on the steady flow rig. Using this data and the valve lift / crank angle relationship, the constant pressure drop on the steady flow rig for an engine speed of 1000 rpm was found to be 64mm/H_2O.

INLET VALVE CURTAIN VELOCITY PROFILES - During the presentation of the results, reference will be made to valve I and II. Valve I is nearest the tumble to swirl conversion tube, whilst valve II is the valve furthest away from the conversion tube.

Figures 7 to 12 show the intake valve curtain profiles for the shrouded valve disc head (200mm/H_2O), sleeved and non-sleeved pent roof chamber at 8mm valve lift. The results are plotted as component vectors of the resultant mean velocity, resolved in the radial/ tangential direction, and the radial/axial direction.

The four valve pent roof configurations were both operated at a constant pressure drop of 64mm/H_2O, which simulates an engine speed of 1000rpm. A direct comparison can therefore be made between the intake valve curtain profiles for the no ramps and 30mm ramps inserted. The velocity measurements for both valves confirm that there is relatively more flow being forced over the top of the valves with the 30mm ramps inserted than for no ramps inserted. It is also interesting to note that there is a swirling structure around each valve periphery with the 30mm ramps inserted.

It is not possible to draw a direct comparison in terms of velocity magnitude with the results conducted on the shrouded valve disc head due to the different pressure drop, however the basic trends can be analysed. It is interesting to note that there is no evidence of any swirling flow around the valve periphery, as was observed with the pent roof chamber with the 30mm ramps inserted. This may be due to the relative orientation of the intake ports parallel to the mid-plane between the valves.

The intake valve profiles for valve I and II of the pent roof chamber are more similar than for the shrouded valve disc head. The differences on the shrouded valve disc head are likely to be an effect of the presence of the tumble to swirl conversion tube. This effect is smaller on the pent roof chamber due to the greater relative confinement of the intake valves.

DISCHARGE COEFFICIENT - In order to assess whether incorporating the ramps affected the breathing capacity of the engine, it was necessary to calculate the discharge coefficient, C_d. This is defined as the ratio between the measured mass flowrate (m) through the inlet ports for a constant pressure drop at each valve lift, to the isentropic

mass flowrate (m_i) through a nozzle with a throat area equal to the inlet valve curtain area and for the same pressure drop, i.e

$$C_4 = \frac{m}{m_i}.$$

where.

$$\dot{m}_i = A_L \left(\frac{P}{P_0}\right)^{\frac{1}{\gamma}} \sqrt{\frac{2\gamma}{\gamma - 1} P_0 \rho_0 \left[1 - \left(\frac{P}{P_0}\right)^{\frac{\gamma-1}{\gamma}}\right]}$$

where.γ = Ratio of specific heats for air taken to be 1.4.

ρ_0 = Density of air at ambient temperature and pressure (kg/m^3).

P = Downstream static pressure in the cylinder (N/m^2).

P_o = Upstream stagnation pressure (N/m^2).

A_l = Inlet valve curtain area (m^2).

Figures 13 and 14 show that the discharge coefficient (C_d) remains unaffected above a pressure drop of 200mm/H_2O at all valve lifts for no ramps and 30mm ramps inserted in the pent roof chamber. This shows that the discharge coefficient is insensitive to pressure drop above this figure.

Figure 15 shows the variation of the discharge coefficient for various valve lifts at 64mm/H_2O pressure drop for the cylinder head with no ramps and 30mm ramps inserted. The most important observation is that there is a reduction in C_d with the addition of the 30mm ramps. This observation shows that the ramps restrict the breathing capacity of the engine. One possible reason for the increase at low valve lifts could be due to flow reattachment to the valve seat allowing an increase in the effective flow area and hence an increase in the discharge coefficient[10].

CONVERSION TUBE SWIRL AND AXIAL VELOCITY PROFILES - The experimental procedure is similar to that presented by Arcoumanis in 1993 [5]. He conducted swirl measurements at the three bore measuring plane for various valve lifts and computed a tumbling vortex ratio (TVR. defined later) at IVC. In this study, the single component LDA system was used to determine the swirl and axial velocity measurements at the one, two and three bore measuring plane. Swirl measurements are also conducted within the cylinder.

EFFECT OF PRESSURE DROP - To determine whether the experimental technique was applicable to pressure differences above 64mm/H_2O, the pressure drop across the test section was raised to 215mm/H_2O.

Figure 16 shows the effect of pressure drop on the swirl velocity profiles at 2 and 9mm valve lifts at the three bore measuring plane for no ramps inserted. The results shown are non-dimensionalised by simulated mean piston speed (2.97 and 5.93m/s respectively) to enable a direct comparison of the results. It can be seen that the differences between both 2 and 9mm valve lifts are preserved for both pressure drops. This observation indicates that when normalised by the simulated mean piston speed the experimental technique can be applied to pressure drops exceeding 64mm/H_2O across the test section.

SWIRL VELOCITY PROFILES - Figures 17 and 18 show a comparison of the swirl velocity profiles for all three cylinder head configurations at 8mm valve lift at the three bore measuring plane.

The most important observation is that the swirl magnitudes are the highest for the shrouded valve disc head, and intermediate and low for the pent roof chamber with 30mm ramps and no ramps inserted respectively. These observations are also consistent with the intake valve curtain velocity measurements. For both the high and intermediate swirling cases, the magnitude of the velocity on both sides of the tube remain approximately constant towards the wall. This effect is thought to be due to the friction of the walls retarding the flow in this region. In both cases the central region exhibits a more solid body rotation type flow.

AXIAL VELOCITY PROFILES - Figures 19 and 20 show a comparison of the axial velocity profiles for all three cylinder head configurations at 8mm valve lift.

The most prominent differences are

1. For the shrouded valve head the flow pattern has high velocities in the wall region and lower velocities near to the centre of the conversion tube.

2. For the pent roof chamber with the 30mm ramps inserted, the flow is higher on one side of the conversion tube, decreasing to a minimum value on the other side.

3. For the pent roof chamber with no ramps inserted, the axial velocity profiles are relatively constant.

The higher velocities observed near the walls for the higher swirling heads may be explained by the fact that within the cylinder, most of the incoming flow impinges on the cylinder walls and travels as a wall jet into the conversion tube. A higher degree of swirl will execute more revolutions per unit length of conversion tube than lower degrees of swirl. This is analogous to a spring which is compressed at high swirls, and becomes more elongated as the swirl level reduces. Hence, the corresponding axial velocity profile will exhibit the features explained in 1 to 3. It is also interesting to note that for the higher swirling case there is a region of reverse axial flow near the centre of the tumble to swirl conversion tube. This may, cause the swirl to process with time and distance [11].

TUMBLING RATIO CALCULATIONS - To define the degree of tumble produced by the various cylinder heads, the tumbling vortex ratio at inlet valve closure (TVR_o) was calculated according to the procedure developed by Arcoumanis in 1993 [5]. This is defined as the ratio between the angular velocity of an equivalent solid body rotating to the crankshaft rotational speed. The former was calculated by integrating NRT (see below) over the valve lift period using the flow coefficient and the relationship between the valve lift and crank angle relationship for the camshafts provided.

The non-dimensional tumbling coefficient (NRT) is defined as the ratio between the angular momentum flux and the axial momentum flux of the flow at the measuring plane normalised by cylinder bore. The angular momentum flux was calculated at the various valve lifts from the vertical and horizontal swirl velocity profiles measured at the three bore measuring plane.

Figure 21 shows plots for the NRT versus valve lift for no ramps inserted and 30mm ramps inserted for the four valve pent roof chamber. It can be seen that the magnitudes of the NRT's for the 30mm ramps inserted are higher at valve lifts of 4, 6, and 8mm. The scatter observed

for no ramps inserted is due to the difficulties in determining the swirl centre for low degrees of tumble. It was found that the tumbling vortex ratio at intake valve closure for the medium tumbling head was approximately 1.4, and for the high tumbling head was 2.5. The TVR for the low tumbling head was not calculated due to the inability to accurately define the swirl centre which will lead to inaccurate values.

The method employed by Arcoumanis to calculate the TVR, assumes that the axial velocity profile across the diameter of the tumble to swirl conversion tube remains constant. It has been shown (figures 19 & 20) that this is not necessarily the case, so an analysis was also conducted to include the variation of the axial velocity profile across the diameter of the tumble to swirl conversion tube. The TVR for the medium tumbling head increased from 1.4 to 1.7. whilst the high tumbling head altered from 2.5 to 3.1. This highlights the necessity to take precautions when estimating the value of TVR at IVC on steady state flow rigs.

EFFECT OF MEASURING LOCATION - Figure 22 shows a comparison of the swirl velocity profiles in the horizontal plane at the two and three bore measuring locations for the low tumbling configuration. These measurements were conducted at 10mm valve lift. This valve lift is higher than the maximum valve lift of the production engine however, this case was chosen as it exhibited the highest NRT for the low tumbling head.

The major observation is that the zero velocity point does not remain in the same position, but precesses around the central core of the tumble to swirl conversion tube. This observation highlights the necessity to integrate from the flow centre, rather than the cylinder centre when computing non-dimensional tumbling ratios (NRT) and TVR [5].

Figure 23 shows an isometric view of the steady flow rig equipped with the high tumbling shrouded valve disc head at 10mm valve lift, 200mm/H2O. CFD simulations using a commercial code (STAR CD) are superimposed on this figure. A detailed comparison between the experimental data and the CFD predictions has been reported in an earlier paper by the authors [6]. This showed that the axial velocity profiles within a swirling flow could be predicted to a fair degree of accuracy. whilst the swirl velocity correlations were poor in both magnitude and form. Despite this the general trends of the flow predicted by CFD techniques remains consistent with experimental data, and so can be used as a guide to the velocity distributions within the steady flow rig. Figure 24 shows a side view of the velocity distribution taken in a vertical plane of the conversion tube. Figure 23 also indicates that the swirl centre is precessing about the axis of the tumble to swirl conversion tube along its entire length. The predictions shown in figure 24, indicate that flow field exhibits a complex structure along the length of the tumble to swirl conversion tube. Also of note is that there are regions of reverse axial flow within the conversion tube due to the low pressure created at the centre of the swirling vortex. Experimental data for the high swirl head (figures 19 & 20), also shows regions of recirculating flow.

CONCLUSIONS

An experimental and computational study has been undertaken on four valve cylinder heads under steady flow conditions. Three cylinder head configurations were tested which were found to produce high, medium, and low levels of tumble. The following conclusions have been derived from this study:

1. Differing degrees of swirl produce differing axial Velocity profiles within the tumble to swirl conversion tube. In the case of high swirl, reverse axial flow can occur at the swirl centre due to the swirling flow creating a lower pressure at the centre of the vortex.

2. Both experimental results and CFD predictions show that the swirl centre precesses around the central core of the tumble to swirl conversion tube. The swirl centre precession occurs at all levels of tumble generated in this study. This highlights the necessity to integrate the swirl velocity profiles from the flow centre when computing NRT and TVR.

3. The above results indicate that care must be exercised in deducing barrel swirl for real engines from steady flow rig results.

ACKNOWLEDGEMENTS

The authors wish to thank Dr. D.Cuttler and Mr. S.Richardson of Jaguar Cars Ltd. for technical assistance and the supply of the CFD code. Support for this project was provided by the Science and Engineering Research Council (Grant No. GR/44608).

REFERENCES

1. Amann C.A., “The automotive engine - A future perspective” SAE 891666, 1989.

2. Benjamin S.F. “The development of the GTL ‘barrel swirl’ combustion system with applications to four valve spark ignition engines”. Paper C54/88, IMechE. 1988.

3. Kuwahara K., Watanabe T., Omori S., Kume T., Ando H., “Optimisation of in-cylinder flow and mixing for a centre-spark four valve engine employing the concept of barrel stratification”. SAE 930478, 1993.

4. Chapman J., Garrett W.M., Warburton A., “A new standard for barrel swirl movement”. IMechE, AutoTech, C427/18/156. IMechE, 1991.

5. Arcoumanis C., Hu Z. Whitelaw J.H., “Steady flow characterisation of tumble generating four valve cylinder heads”, *Proc. IMechE*, Part D, 1992.

6. Seeley W.A., Baker P., Girgis N.S., Benjamin S.F., “An experimental and predictive study of the tumble generating characteristics of four valve cylinder heads under steady flow conditions”. Seminar paper ‘The validation of computational techniques in vehicle design’ IMechE, 1994.

7. Catania A.E., “Air flow investigation in the open combustion chamber of a high speed four stroke engine”. ASME paper No. 80-FE-5, 1979.

8. Edwards R.V., “Report of the special panel on statistical particle bias problems in laser anemometry”. *Trans of the ASME*, Vol109, 1987.

9. Newman A.W., “A study of the flow field in engines prior to ignition”, PhD Thesis, Coventry University, 1994.

10. Bicen A.F., Vafidis C., Whitelaw J.H., “Steady and unsteady air flow through an intake valve of a reciprocating engine”. Journal of Fluids Engineering Vol 107/413, 1985.

11. Arcoumanis C., Hadjiapostolou A., Whitelaw J.H., “Swirl centre precession in engine flows”. SAE 870370, 1987.

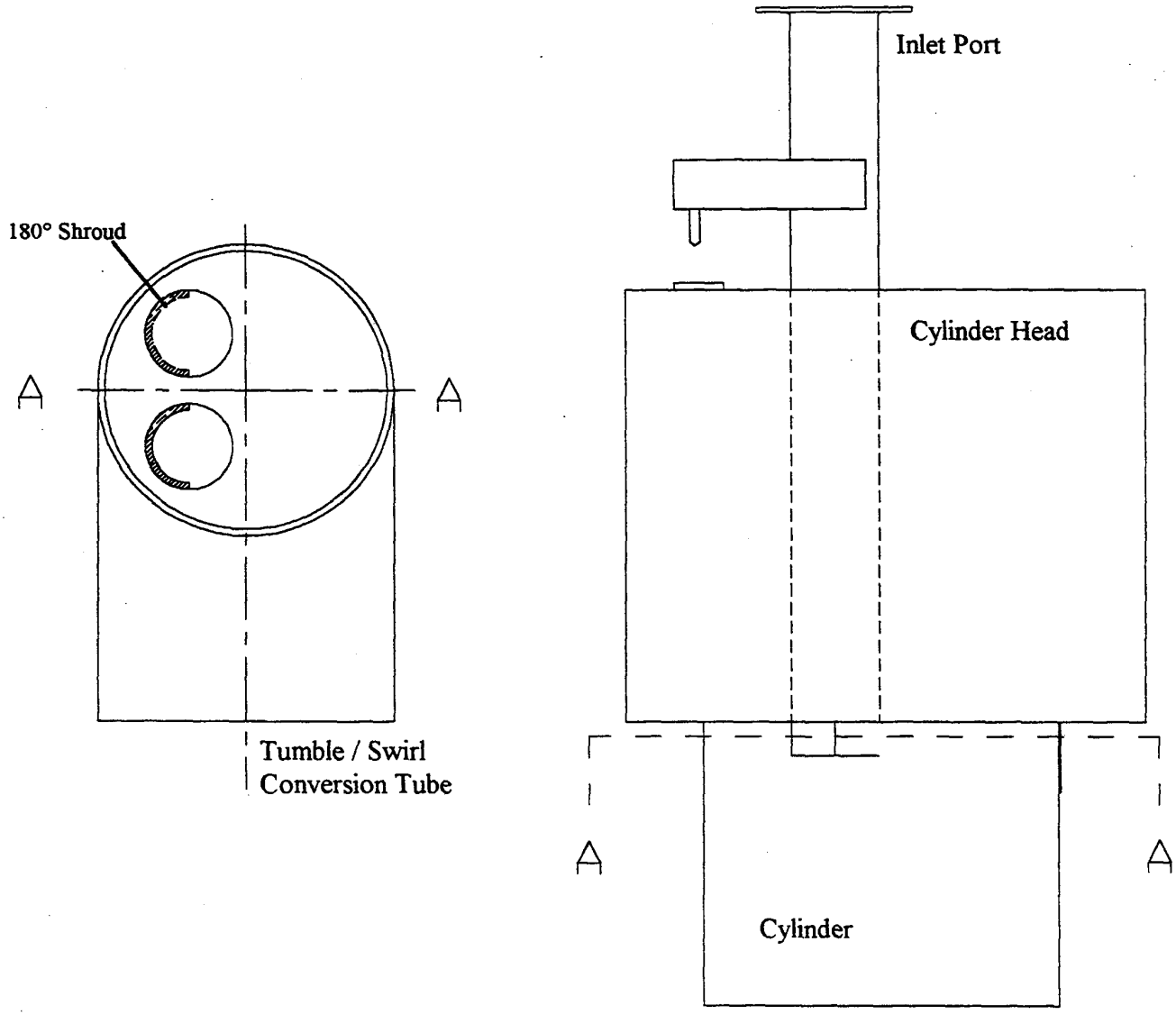

Fig. 1 - Shrouded valve disc head.

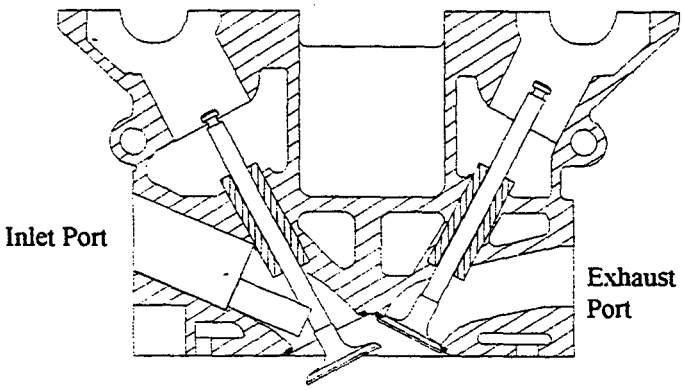

Fig. 2 - Four valve pent roof chamber configuration.

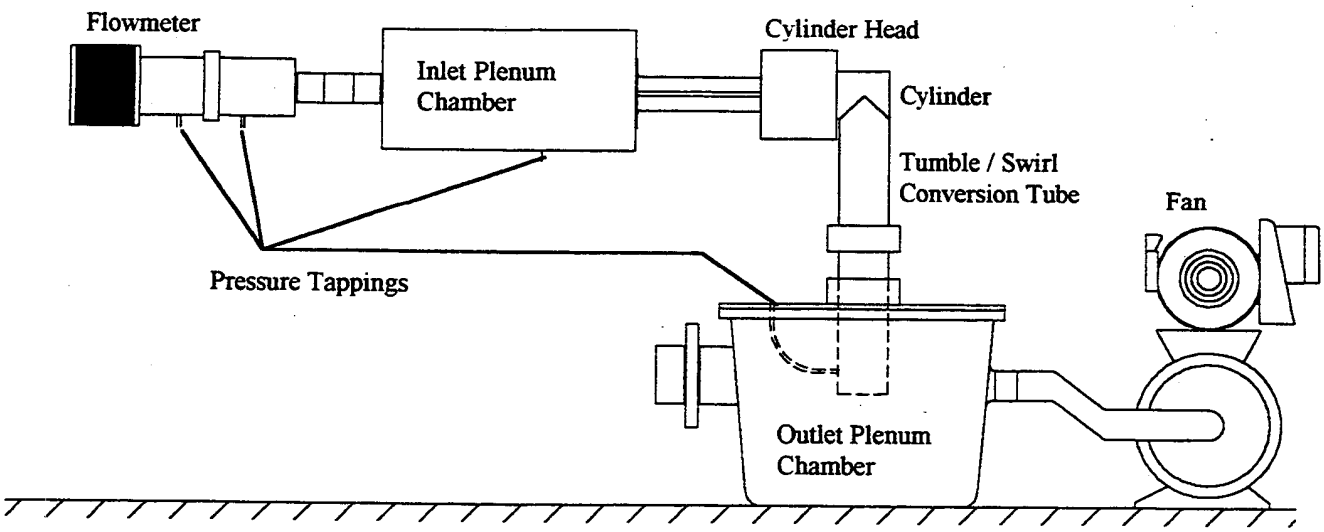

Fig. 3 - Steady state flow rig schematic.

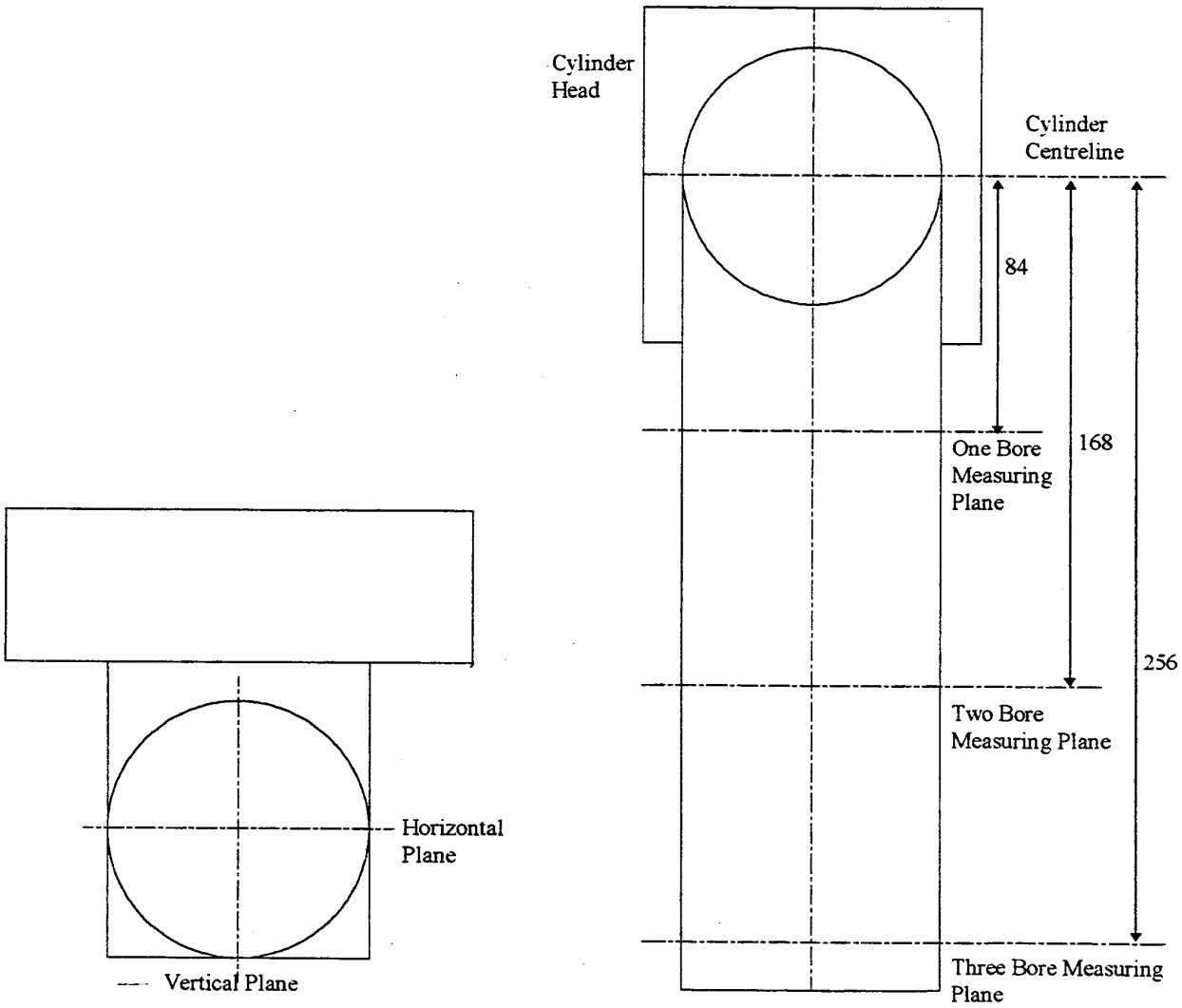

Fig. 4 - Measuring location for LDA measurements.

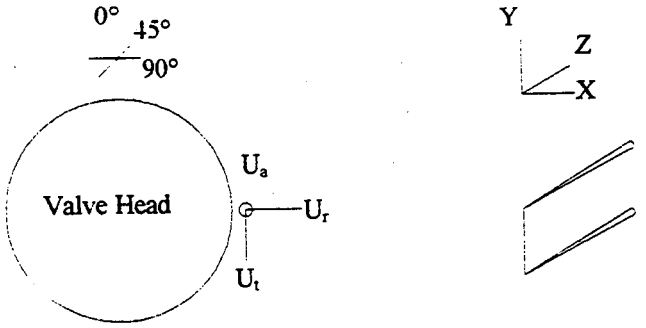

Fig. 5 - HWA resolving orientations.

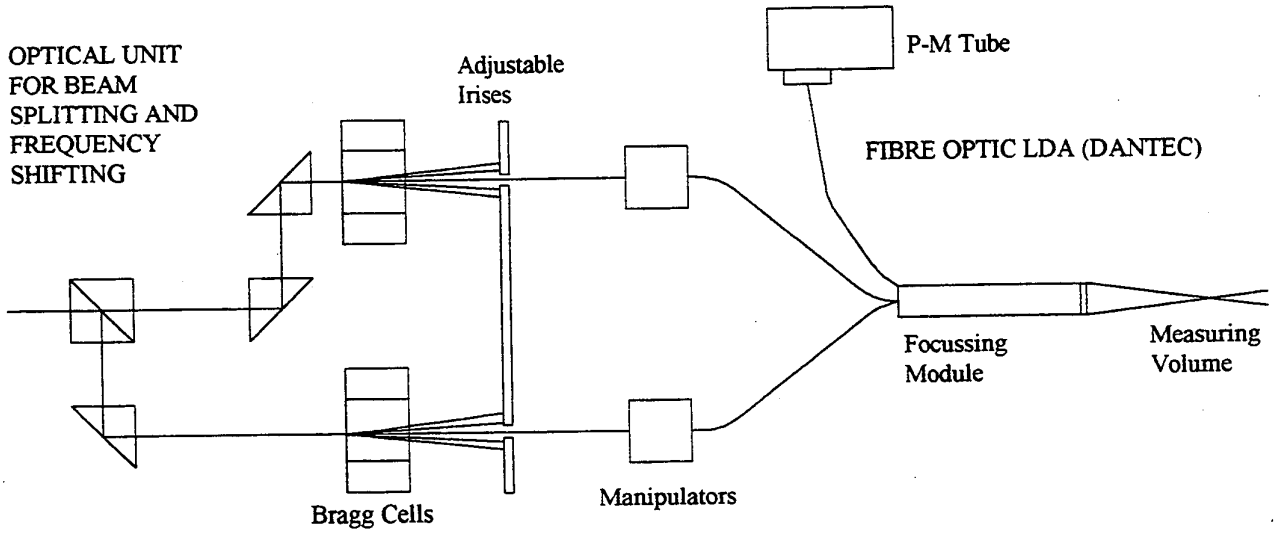

Fig. 6 - Arrangement of LDA system.

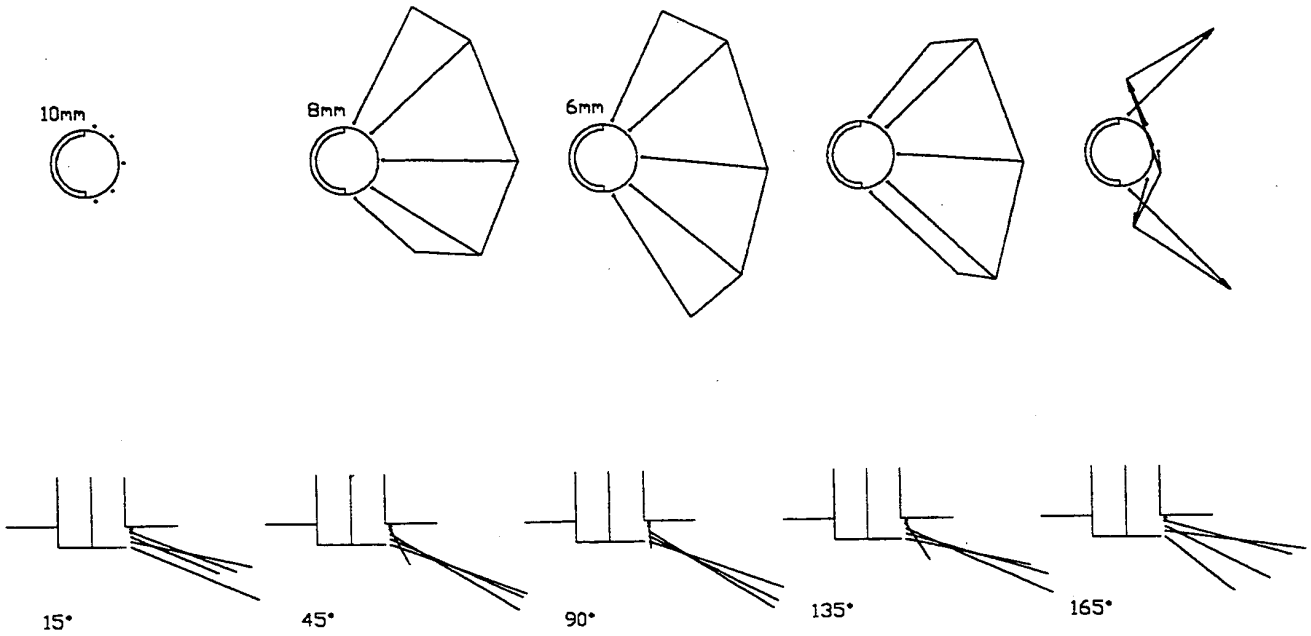

Fig. 7 - Disc head inlet valve velocity profiles, valve I.

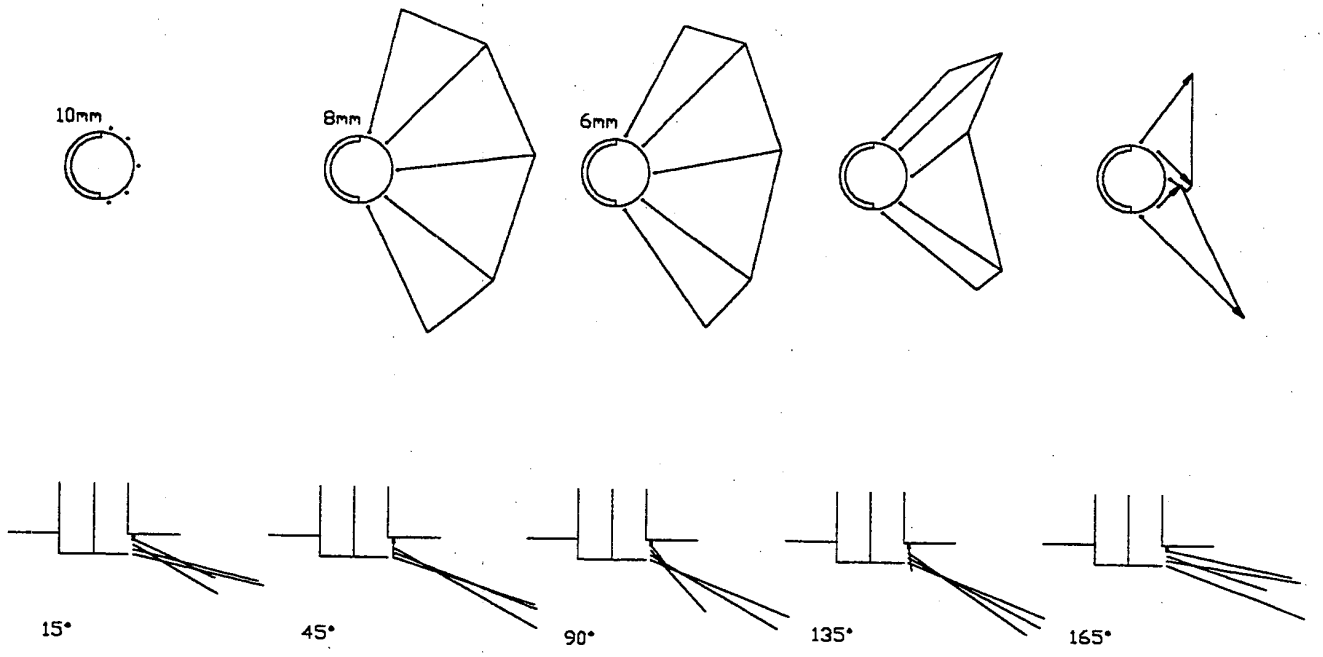

Fig. 8 - Disc head inlet valve velocity profiles, valve II.

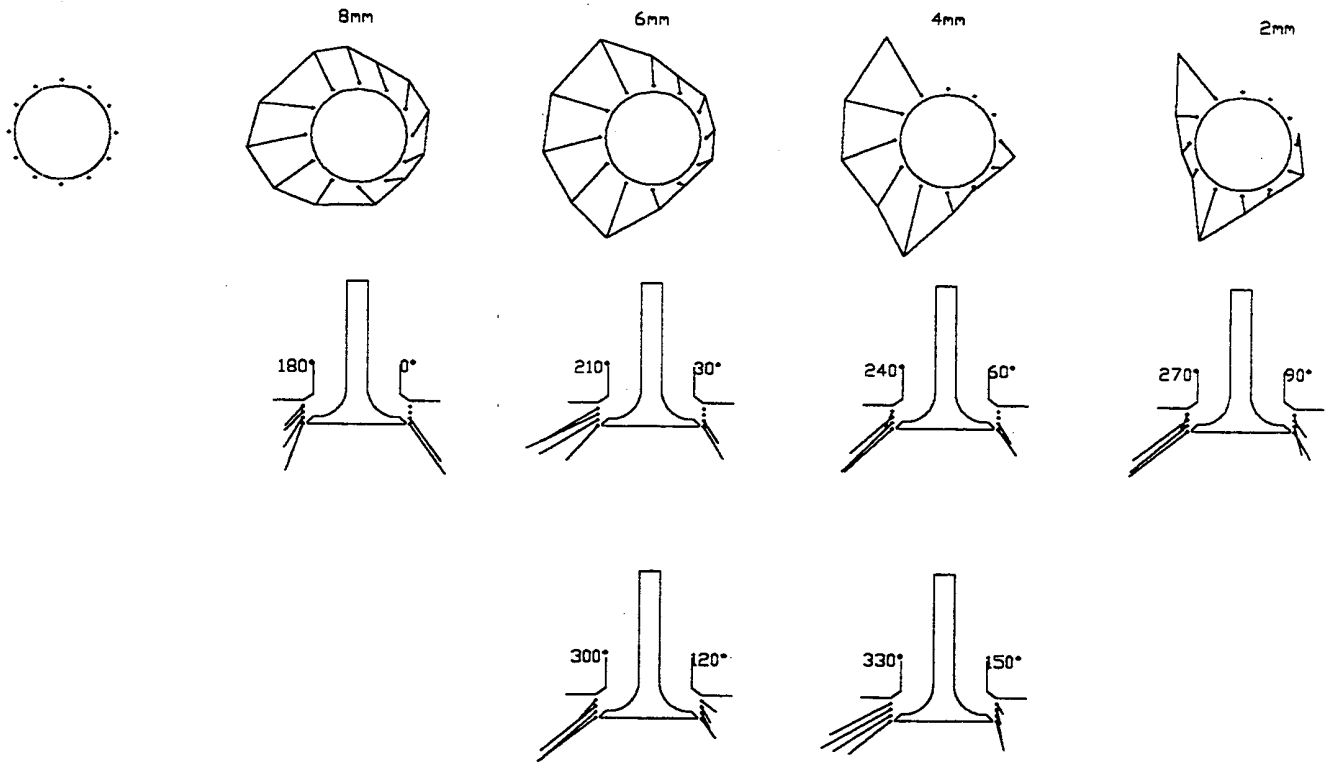

Fig. 9 - Pent roof head with 30mm ramps inserted, inlet valve velocity profiles, valve I.

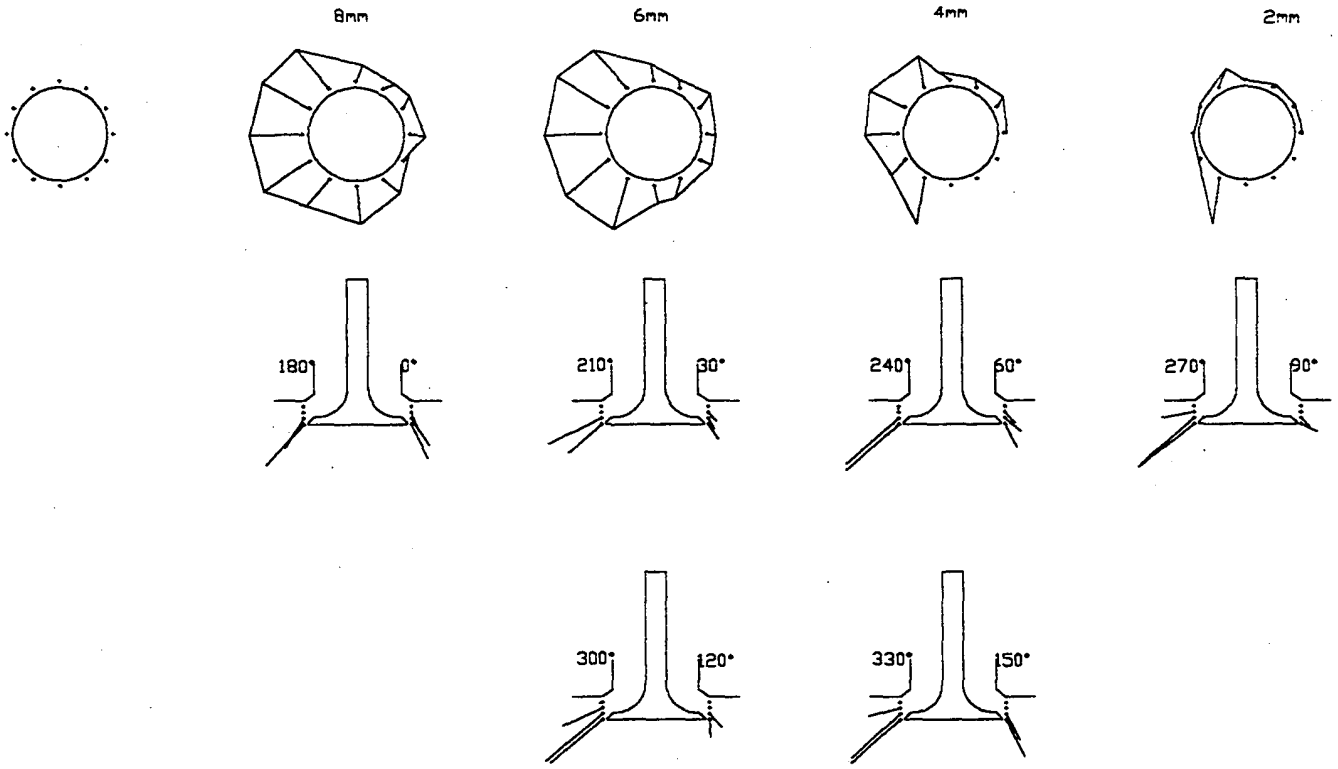

Fig. 10 - Pent roof head with 30mm ramps inserted, inlet valve velocity profiles, valve II.

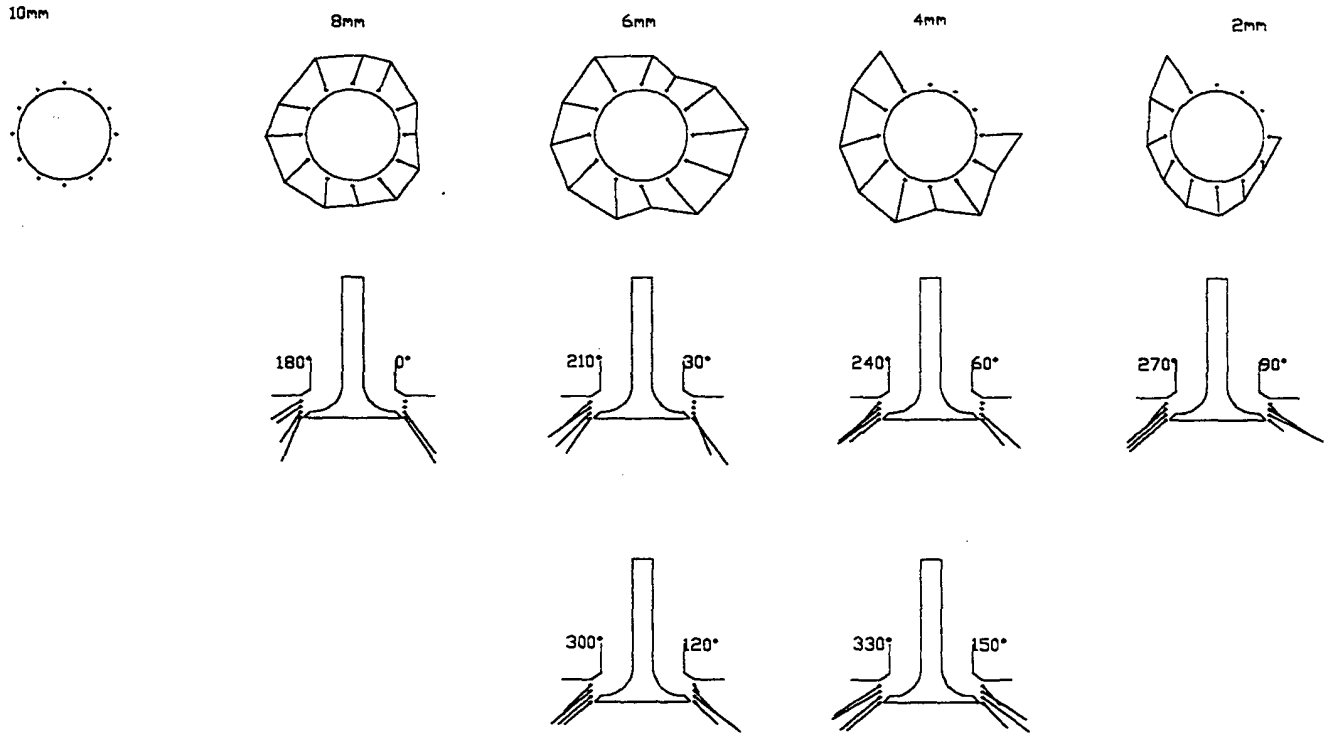

Fig. 11 - Pent roof head with no ramps inserted, inlet valve velocity profiles, valve I.

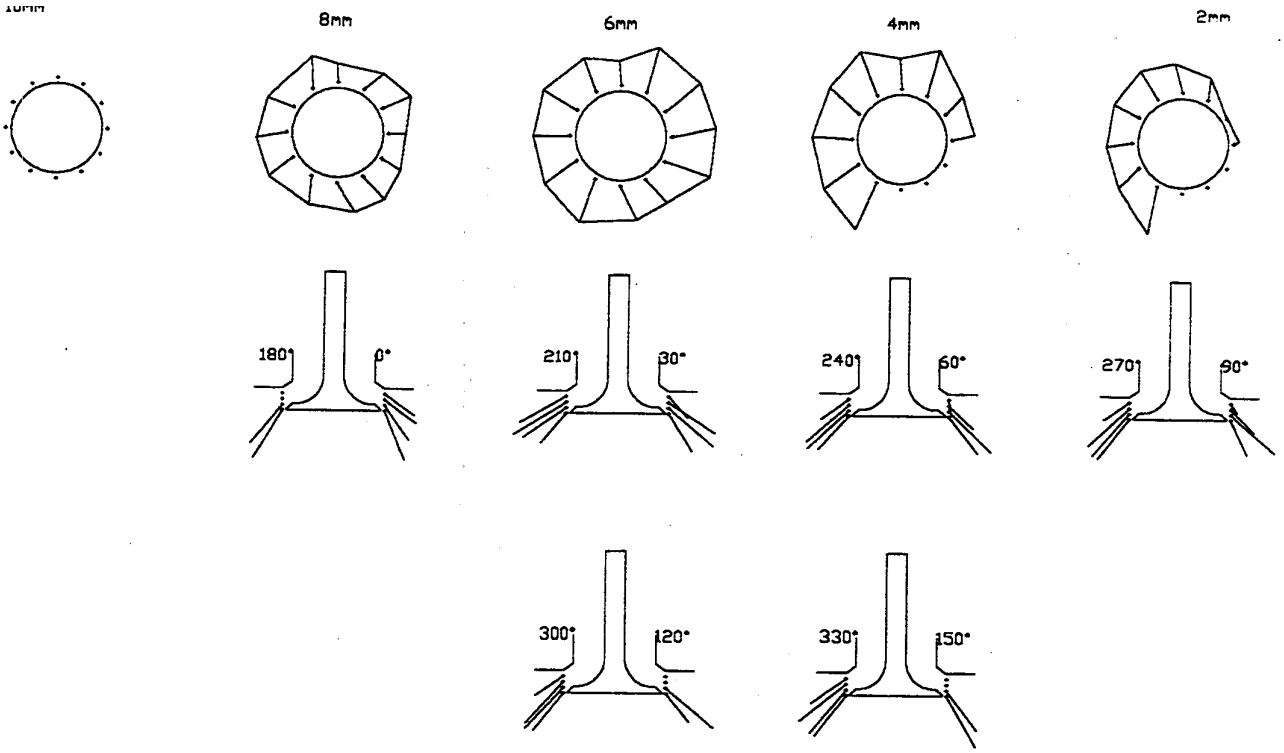

Fig. 12 - Pent roof head with no ramps inserted, inlet valve velocity profiles, valve II.

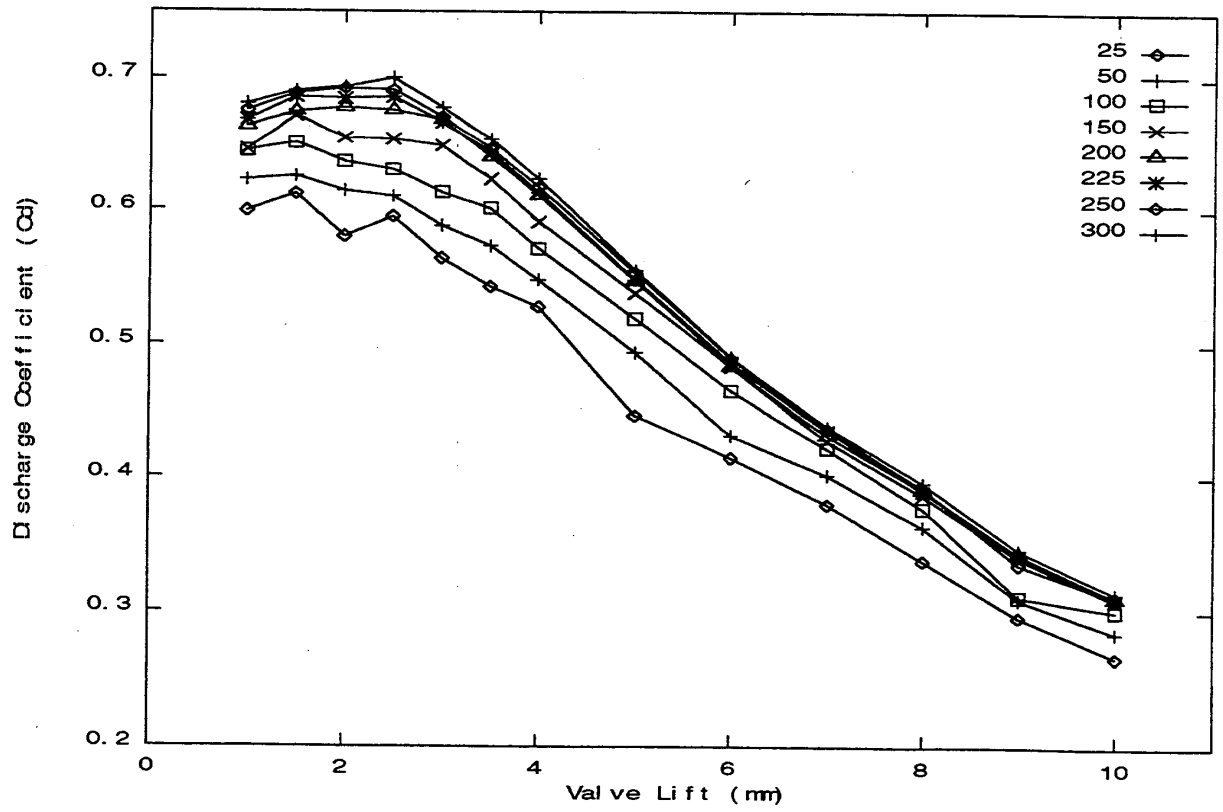

Fig. 13 - Discharge coefficient for various pressure drops (mm/H_2O), low tumbling cylinder head.

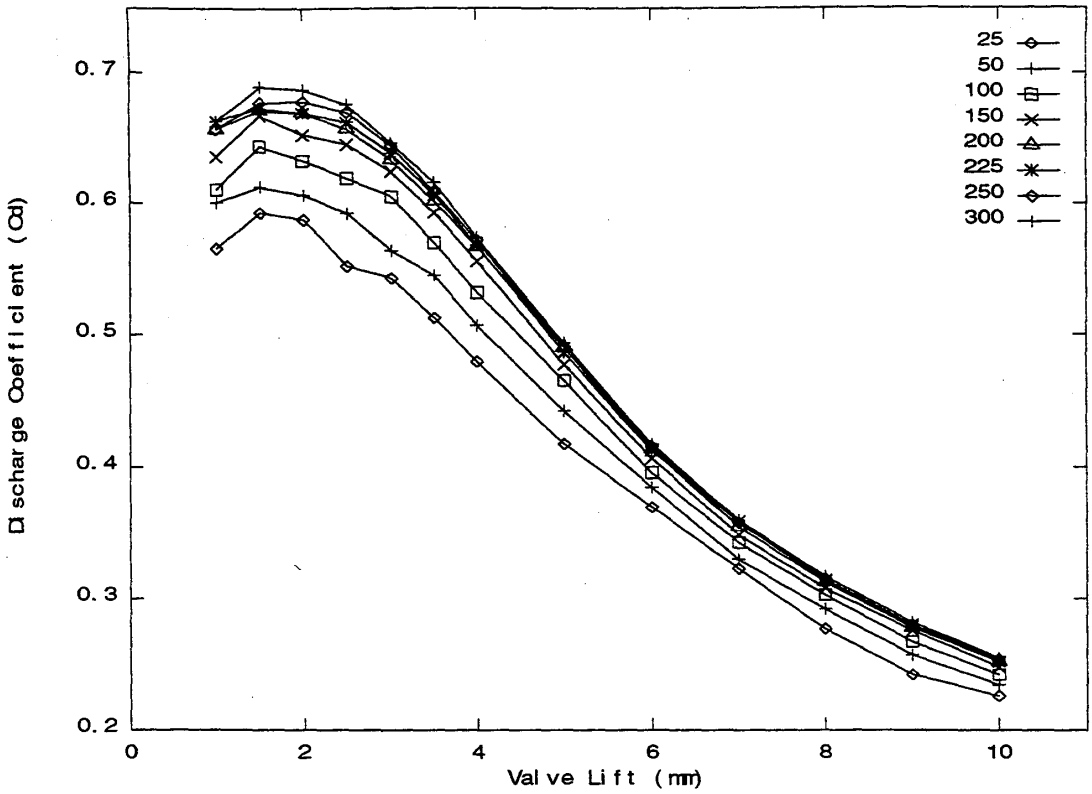

Fig. 14 - Discharge coefficient for various pressure drops (mm/H_2O), medium tumbling head.

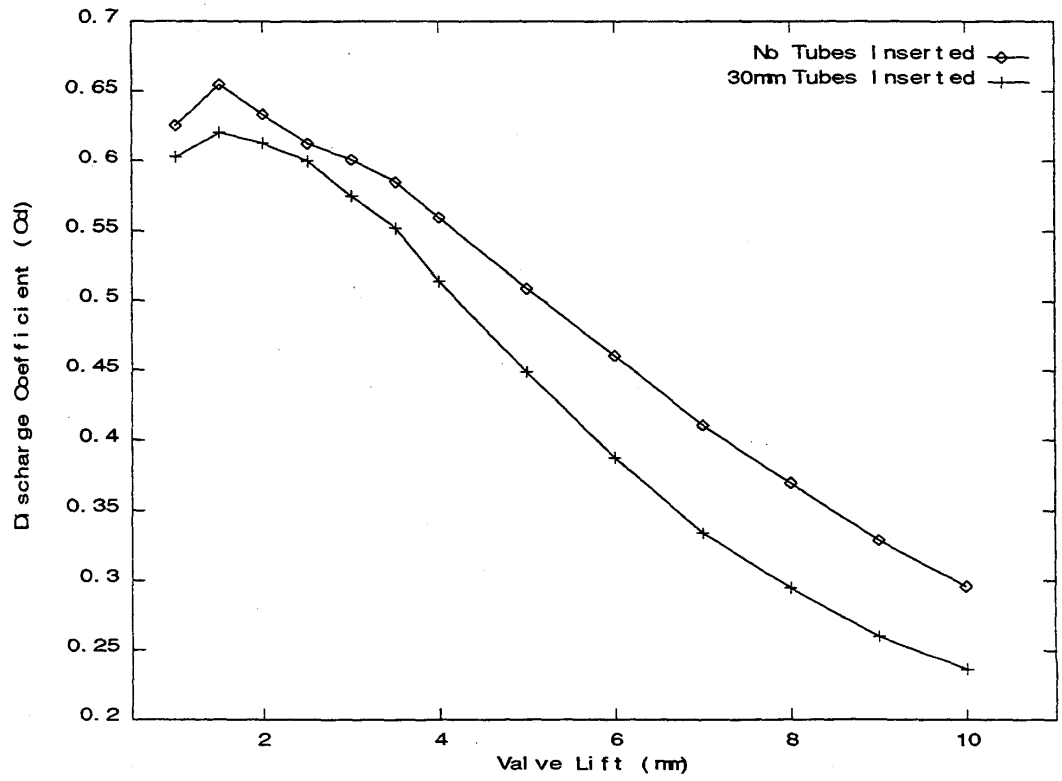

Fig. 15 - Discharge Coefficients for pent roof chamber.

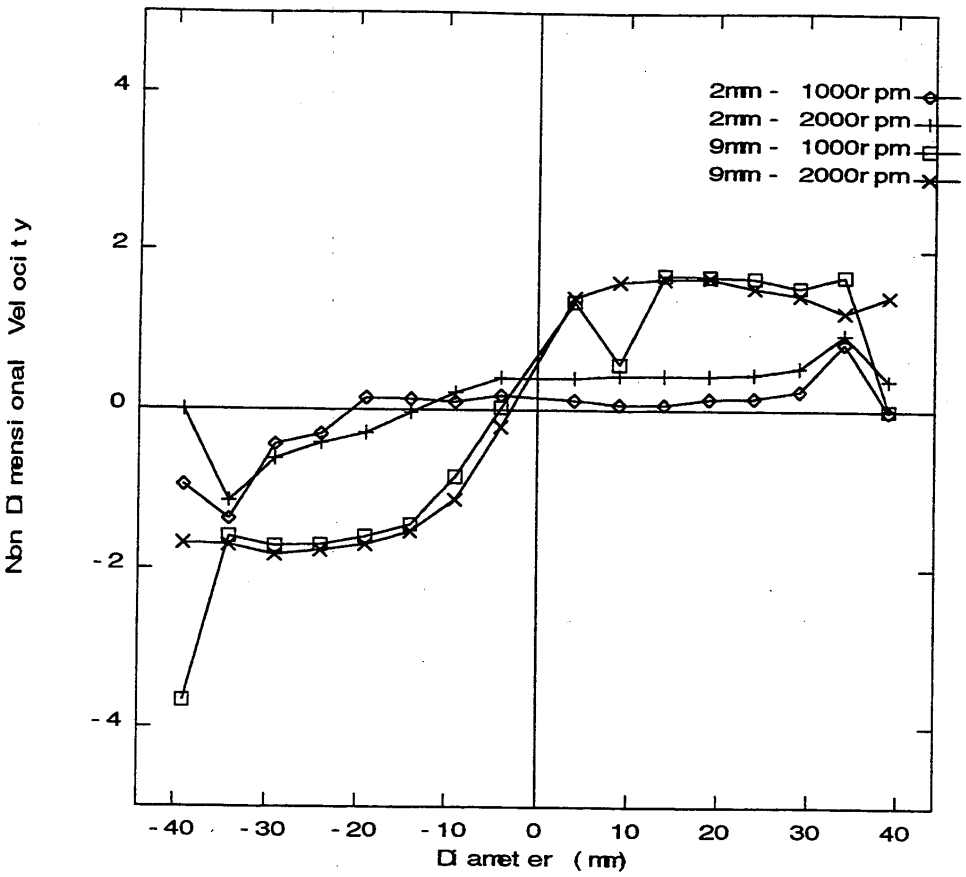

Fig. 16 - Effect of 'engine speed' on low tumbling head.

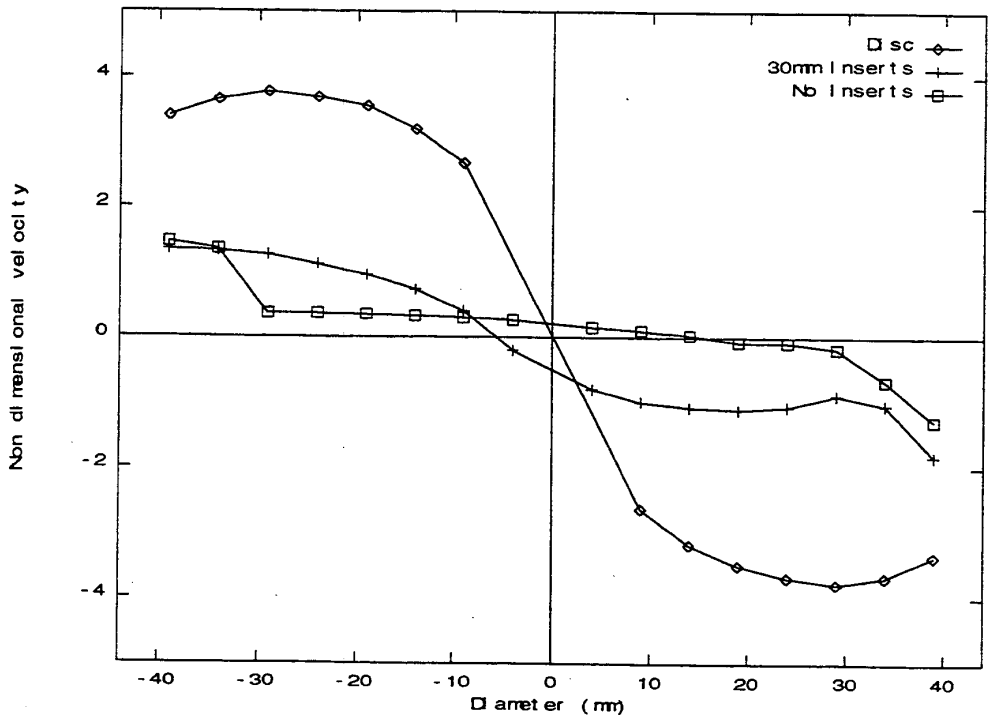

Fig. 17 - Swirl velocity Profiles, 8mm valve lift, horizontal plane.

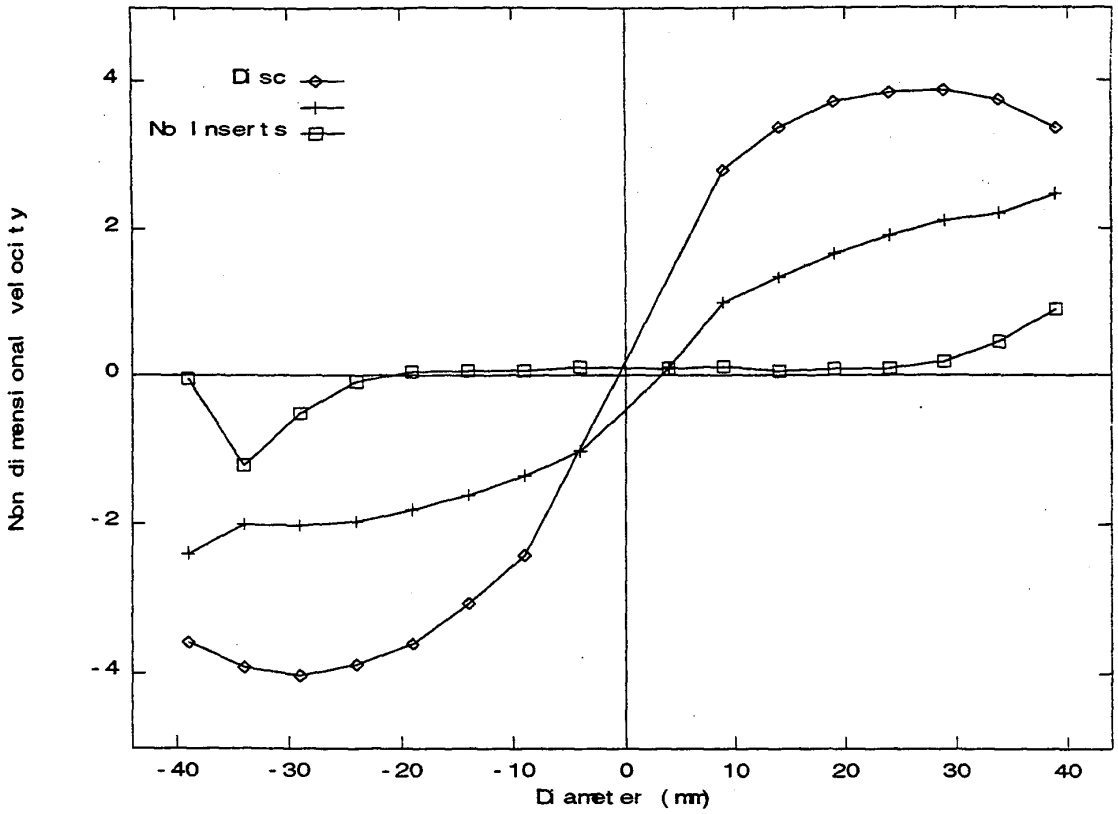

Fig. 18 - Swirl velocity profiles, 8mm valve lift, vertical plane.

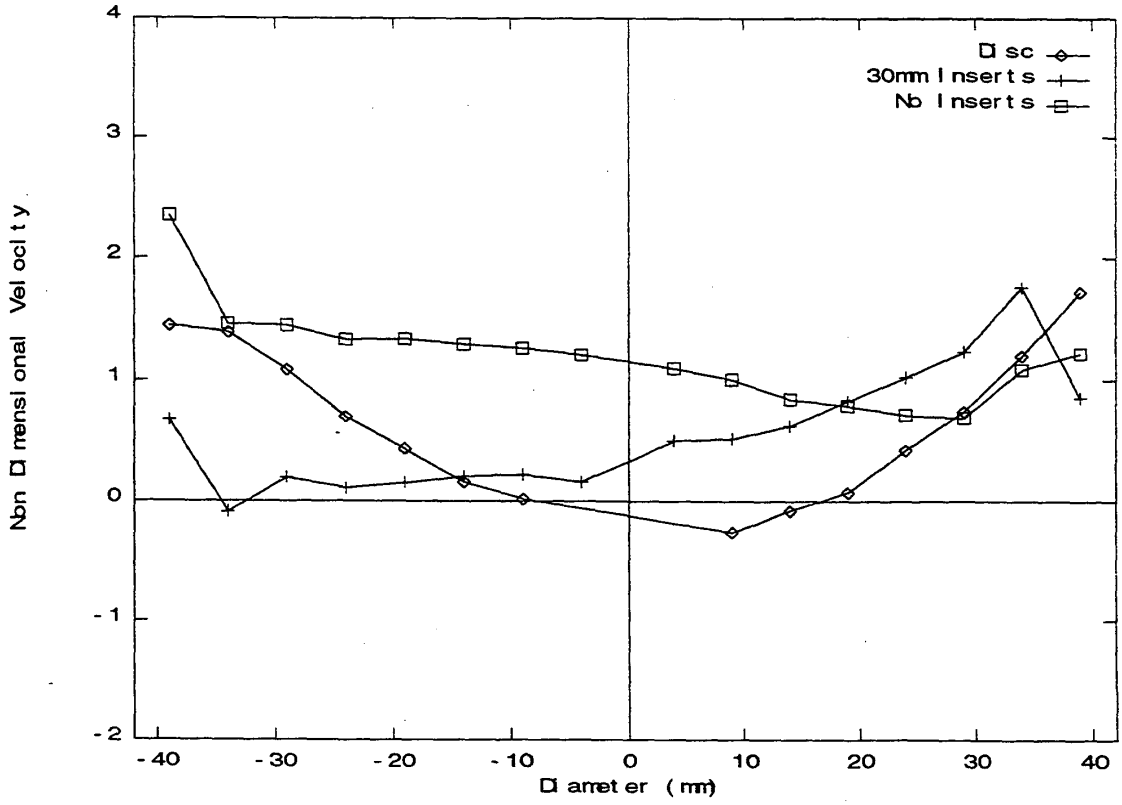

Fig. 19 - Axial velocity profiles, 8mm valve lift, horizontal plane.

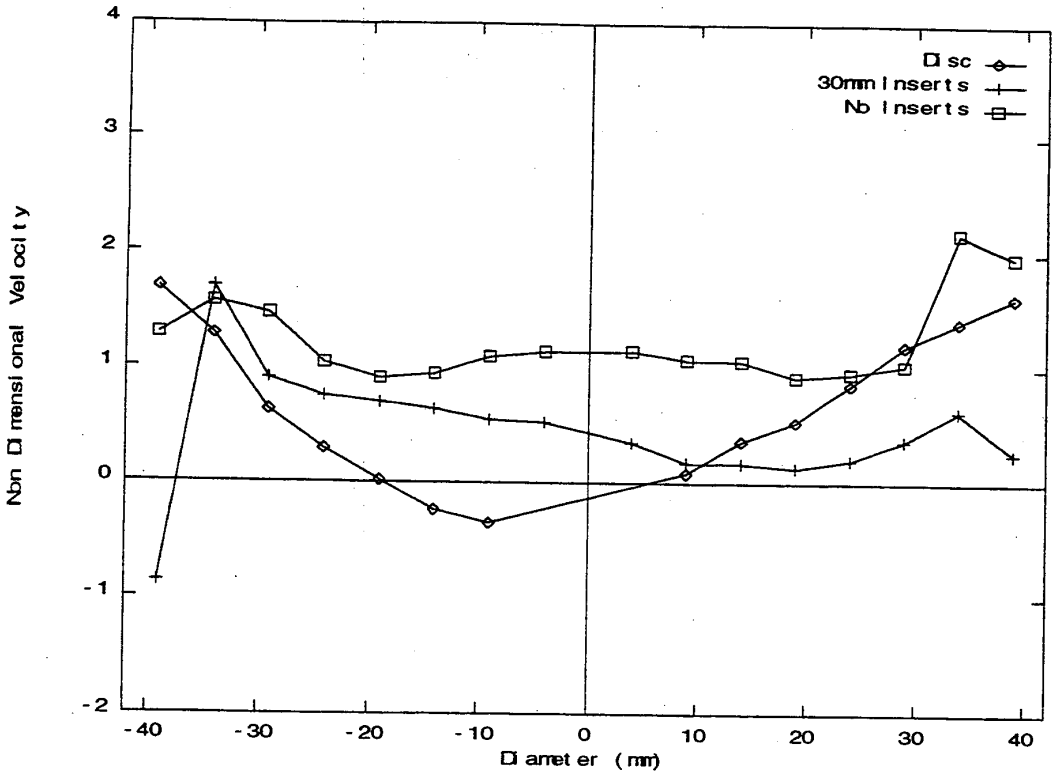

Figure 20 - Axial velocity profiles, vertical planes, 8mm valve lift.

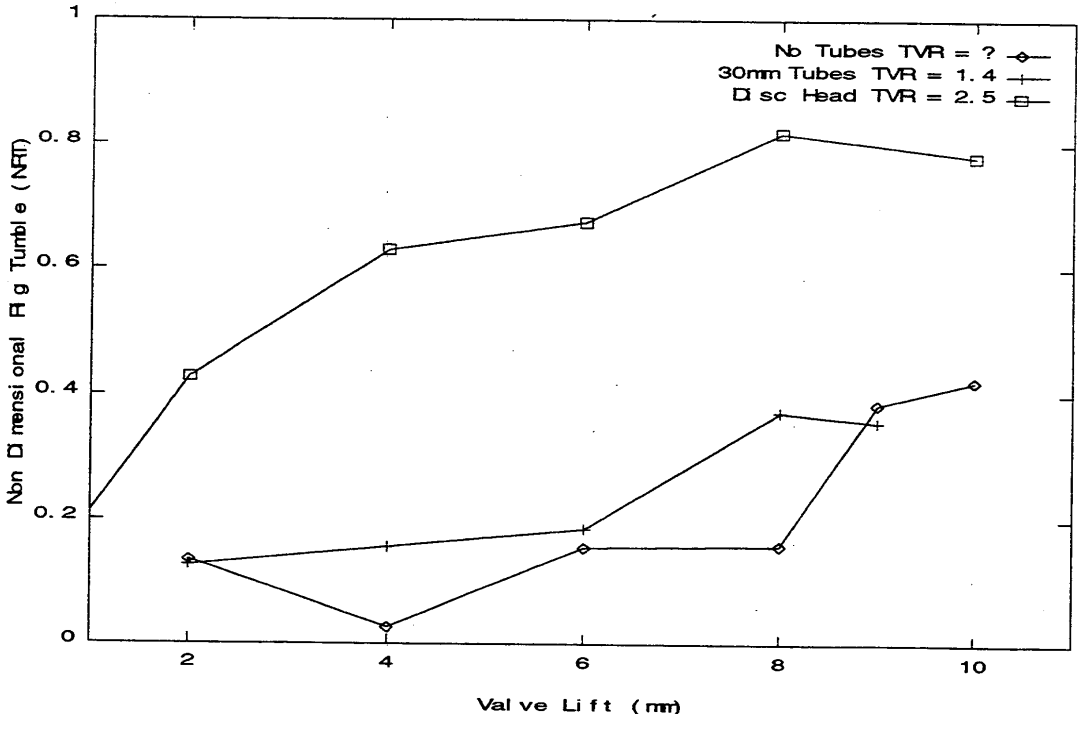

Fig. 21 - Non dimensional rig tumble (NRT).

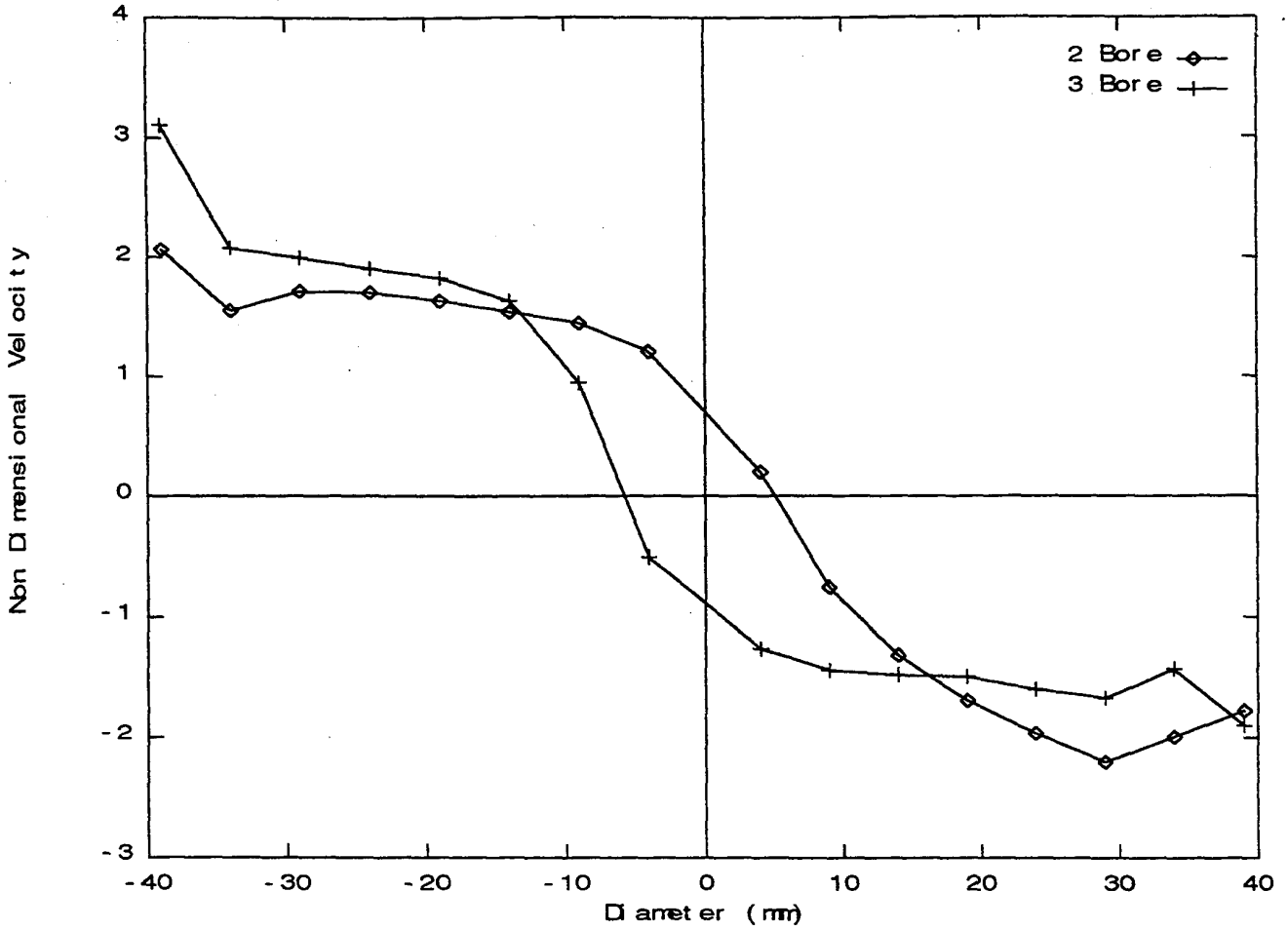

Fig. 22 - Effect of measuring location on the swirl velocity profiles.

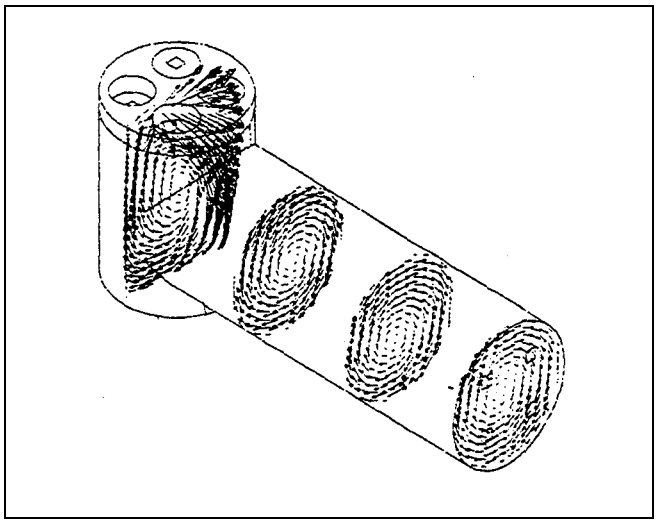

Fig. 23 - Swirl centre precession on high tumbling head, 10mm valve lift.

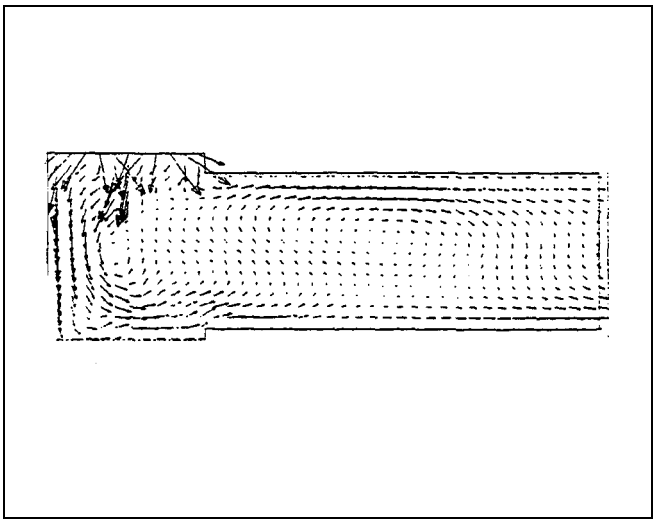

Fig. 24 - Velocity distributions along the length of the tumble to swirl conversion tube.